MIT Open Access Articles

Explorations of Atmosphere–Ocean–Ice Climates on an Aquaplanet and Their Meridional Energy Transports

Explorations of Atmosphere–Ocean–Ice Climates on an Aquaplanet and Their Meridional Energy Transports

DANIEL ENDERTON AND JOHN MARSHALL

Massachusetts Institute of Technology, Cambridge, Massachusetts

ABSTRACT

The degree to which total meridional heat transport is sensitive to the details of its atmospheric and oceanic components is explored. A coupled atmosphere, ocean, and sea ice model of an aquaplanet is employed to simulate very different climates—some with polar ice caps, some without—even though they are driven by the same incoming solar flux. Differences arise due to varying geometrical constraints on ocean circulation influencing its ability to transport heat meridionally. Without complex land configurations, the results prove easier to diagnose and compare to theory and simple models and, hence, provide a useful test bed for ideas about heat transport and its partition within the climate system. In particular, the results are discussed in the context of a 1978 study by Stone, who argued that for a planet with Earth's astronomical parameters and rotation rate, the total meridional heat transport would be independent of the detailed dynamical processes responsible for that transport and depend primarily on the distribution of incoming solar radiation and the mean planetary albedo. The authors find that in warm climates in which there is no ice, Stone's result is a useful guide. In cold climates with significant polar ice caps, however, meridional gradients in albedo significantly affect the absorption of solar radiation and need to be included in any detailed calculation or discussion of total heat transport. Since the meridional extent of polar ice caps is sensitive to details of atmospheric and oceanic circulation, these cannot be ignored. Finally, what has been learned is applied to a study of the total heat transport estimated from the Earth Radiation Budget Experiment (ERBE) data.

1. Introduction

The transport of energy from the tropics toward the poles is a key aspect of the climate system, warming high latitudes and cooling low latitudes. It is hence intimately connected with the equator–pole temperature gradient, a fundamental feature of the climate system. Estimates show that the meridional distribution of poleward total heat transport[1] H_T is remarkably antisymmetric about the equator, peaking at ~5.5 PW at 35° in both hemispheres; see Fig. 1 (Trenberth and Caron 2001, hereafter TC01; Wunsch 2005, hereafter W05). Ocean heat transport H_O makes a large contribution to the total in the tropics, whereas atmospheric heat transport H_A dominates in middle and high latitudes.

Recently, attention has been focused on understanding what sets the partition of heat transport between the atmosphere and ocean and its meridional distribution (Held 2001; Czaja and Marshall 2006; Marshall et al. 2007). Temporal changes in this partition have long been thought to be a productive way of considering climate variability (Bjerknes 1964; Marshall et al. 2001). The possibility that decreased Northern Hemisphere H_O from a weakened Atlantic meridional overturning circulation might trigger abrupt change has also been discussed, raising the question of how H_A might compensate were this to occur (Broecker 1997; Bryden et al. 2005; Wunsch and Heimbach 2006). Important to all of these discussions is an understanding of the influence of the detailed mechanisms of atmospheric and oceanic heat transport in setting H_T, whether it be the ocean's meridional overturning circulation, the Hadley circulation, or atmospheric eddies.

---

[1] Here the common phrase "heat transport" is used synonymously with "energy transport", although it should be remembered that heat is not a fluid property that can be transported: see Warren (1999) for a discussion of terminology.

Corresponding author address: Daniel Enderton, Department of Earth, Atmosphere and Planetary Sciences, Massachusetts Institute of Technology, 77 Massachusetts Avenue, 54-1511A, Cambridge, MA 02139.
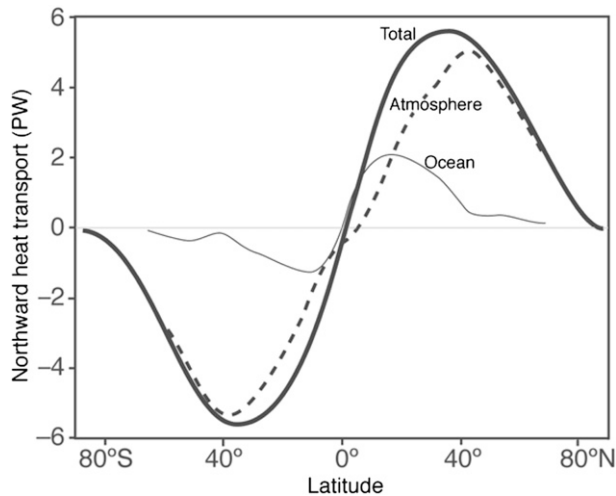E-mail: enderton@mit.edu

FIG. 1. Estimates of total meridional heat transport and its partition between the atmosphere and ocean redrawn from TC01.

To better study the total heat transport of the climate system and its partition between the two fluids, in section 2 we introduce a series of primitive equation atmosphere–ocean–ice calculations to explore the climates resulting from highly idealized geometrical constraints on ocean heat transport. In addition to the pristine aquaplanet (Aqua hereafter) presented in Marshall et al. (2007), we explore three additional configurations with a thin (one grid-cell wide) barrier running from pole to pole. One has no gaps in the barrier (Ridge), one has a gap in the tropics (Equatorial Passage, hereafter EqPas), and one has a gap in the Southern Hemisphere (Drake); see Fig. 2. Without complex land distributions, these configurations prove simpler to diagnose and can be more easily compared to theory and simple models. In this manner, they provide a useful test bed for ideas about the atmosphere–ocean–ice climate system and its heat transport. These coupled calculations show that H_T is rather robust under a variety of heat transport partitions provided that the albedo does not change. The H_T is not constant, however, between climates with significantly different extents of ice cover and, hence, different mean and pole-to-equator gradients in planetary albedo.

In section 3 our results are discussed in the context of the Stone (1978, hereafter S78) model for H_T derived from truncated Legendre polynomial expansions of the pertinent radiation budget variables (an equivalent two-box model also gives insights and is briefly described in an appendix). The model illustrates the interplay between H_T and the pole-to-equator gradients in incoming solar shortwave radiation, outgoing longwave radiation, and planetary albedo. Using this model and the radiation budget measurements of Ellis and Vonder Haar

(1976), S78 argued that H_T ought to depend on the equator–pole gradient in incoming solar radiation and the mean planetary albedo but be rather insensitive to the internal details of atmospheric and oceanic circulation. Here it is found that Stone's result provides a useful guide when there is no ice, but not in cold climates with significant polar ice caps and hence strong meridional gradients in albedo. Since the meridional ice extent is sensitive to details of atmospheric and oceanic circulation, these cannot be ignored. Finally we apply the S78 model to the Earth Radiation Budget Experiment (ERBE) data. Discussion and conclusions are found in section 4.

2. Coupled model employing geometric constraints on ocean circulation

A series of fully coupled atmosphere–ocean–ice calculations have been carried out on an aquaplanet in which there is no land but the ocean circulation is subject to various geometrical constraints by the presence of meridional barriers, as shown in Fig. 2. The philosophy behind such a series of experiments is discussed in Marshall et al. (2007) where the pure aquaplanet solution (no barriers) is described in detail. These idealized configurations allow one to investigate the fundamental fluid dynamics of the coupled climate. The solutions are very rich and much can be said about them. Here we choose to describe the basic climatologies of the various configurations and go on to discuss their associated meridional energy transports in the framework of S78.

Aqua is an entirely ocean-covered planet, whereas Ridge has a thin barrier (one grid cell wide) running from pole to pole, confining the ocean in one large basin. There is no orography in any of the calculations presented here—barriers, when present, do not protrude into the atmosphere. EqPas is identical to Ridge but with a gap in the barrier between 20°S and 20°N that allows zonal ocean flow in the tropics but retains gyral flow in middle to high latitudes. Lastly, Drake, with a gap in the barrier south of 40°S, breaks the hemispheric symmetry. By introducing such geometric constraints on ocean circulation, a range of very different climates is realized, providing a useful context in which to study the total heat transport and its partition between the atmosphere and ocean.

Before going on to a description of the equilibrium solutions, we place our study in the context of previous work. Very few calculations of the kind described here have been carried out before. Toggweiler and Bjornsson (2000) and Hotinski and Toggweiler (2003) present coupled calculations in highly idealized geometries but employed an energy balance model for the atmosphere
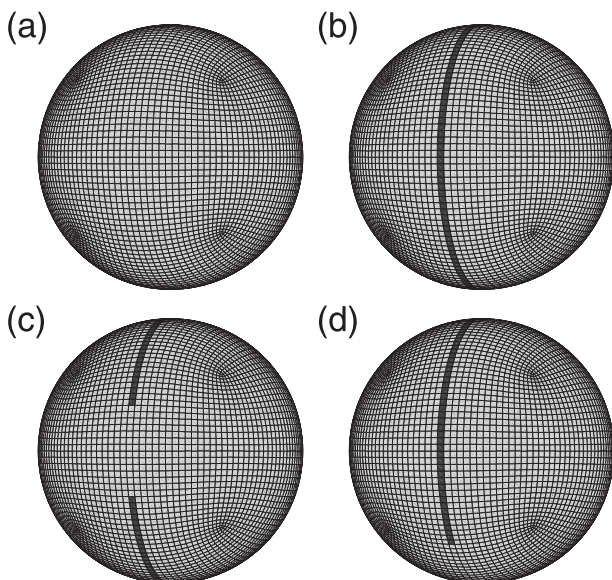
FIG. 2. Position of barriers and gaps in our various aquaplanet configurations: (a) Aqua, (b) Ridge, (c) EqPas, and (d) Drake. Light gray denotes ocean; black, land. Land, when present, comprises a thin strip (one grid cell wide) running in a single 180° arc from pole to pole and does not protrude into the atmosphere. Meridional gaps are introduced in the thin strip of land in EqPas and Drake. Where there is ocean, its depth is a constant 5.2 km with a flat bottom.

with a prescribed surface wind pattern. Smith (2004) describes a coupled aquaplanet system with a dynamical atmosphere coupled to a dynamical ocean. However, the system was not integrated out to equilibrium and the presence of strong lateral diffusive fluxes in the ocean model led to unrealistically large meridional (diffusive) heat fluxes. In contrast to the solutions presented here, all were very warm climates and none maintained ice over the poles.

a. The coupled model

The coupled model used is the Massachusetts Institute of Technology general circulation model (Marshall et al. 1997a,b, 2004). The level of complexity of the model is chosen to provide a balance between the inclusion of key processes while maintaining the necessary computational efficiency to permit synchronously coupled integration for many thousands of years while resolving synoptic-scale eddies in the atmosphere. The atmospheric model has five vertical levels and employs the idealized atmospheric radiation, surface boundary layer, shallow and moist convection, and cloud and precipitation schemes described in Molteni (2003); see also the summary in Marshall et al. (2007). The ocean component has 15 vertical levels spanning 5.2 km and employs the Gent and McWilliams (1990) and Redi

(1982) eddy parameterization schemes as described in Griffies (1998). Diapycnal mixing is represented with a constant vertical diffusivity for temperature and salt of 3×10^{-5} m^2 s^{-1}, somewhat larger than but broadly in accord with observed values of mixing in the ocean thermocline. Owing to our choice of an ocean basin with a flat bottom, topographic form drag plays no role in balancing momentum input from the wind, whereas mountain drag is the primary momentum sink in the Antarctic Circumpolar Current of the present climate. Therefore, to avoid the generation of excessively strong barotropic zonal flows, we employ an enhanced bottom friction (linear drag) parameter that is tuned to damp abyssal currents toward zero. Convection is represented through enhanced vertical mixing, which is treated implicitly as described in Klinger et al. (1996). A two-layer thermodynamic sea ice model based on Winton (2000) is used. The whole system is integrated forward on the cubed sphere (Adcroft et al. 2004) at a horizontal resolution of C32, yielding a grid of roughly 2.8° resolution. The grids used for both atmosphere and ocean are identical, simplifying coupling procedures. Orbital forcing and CO_2 levels are prescribed at present-day values. The seasonal cycle is represented but there is no diurnal cycle. For further details see Marshall et al. (2007).

b. Coupled model climatologies

Here we describe the climatology of the coupled solutions once they have reached equilibrium after 5000 years of synchronous integration. The solutions are not steady and exhibit variability on many time scales—see the discussion of coupling of annular modes in the atmosphere and ocean observed in the Aqua solution in Marshall et al. (2007). We first describe the atmospheric climatologies and go on to discuss the various ocean circulations driven by them that are associated with the various basin geometries. It is important to emphasize that the very different climates realized in this series of experiments are only a consequence of changes in ocean circulation induced by differences in ocean basin geometry.

Figures 3–10 show 20-yr time-averaged climatological fields from the Aqua, Ridge, EqPas, and Drake calculations, employing the idealized geometries shown in Fig. 2. All solutions have an atmospheric zonal-average zonal wind structure in thermal wind balance with the equator–pole temperature gradient, which, in gross structure, is not unlike the present climate (see Fig. 3, top panels). In the tropics there is a Hadley regime with surface easterlies and weak meridional temperature gradients. Strong westerly jets are present in middle latitudes associated with a marked middle-latitude meridional temperature gradient. The surface winds in middle latitudes are westerly. The sense of the surface winds at high
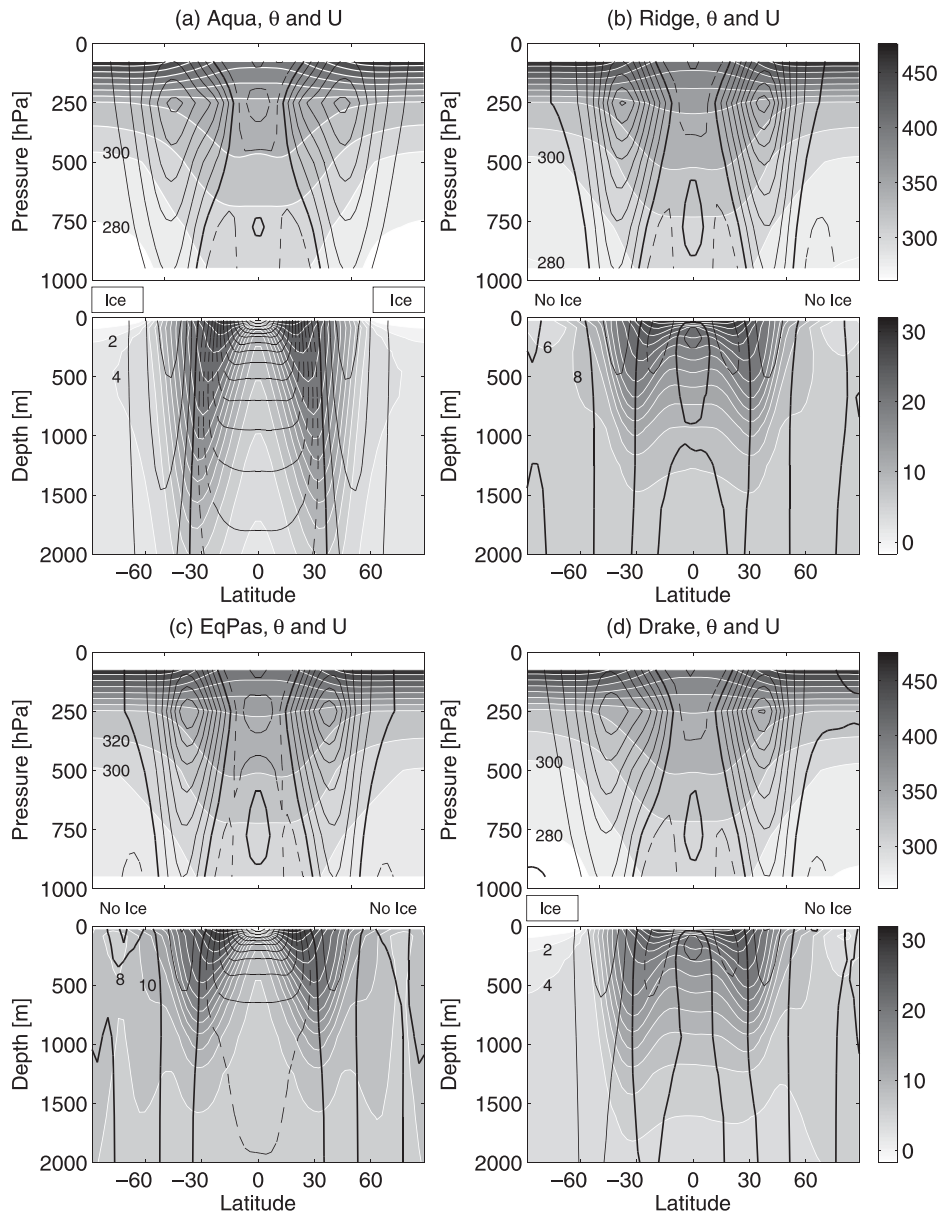
FIG. 3. Twenty-year time and zonal mean potential temperature (shading) and zonal flow (black contours). Atmosphere and ocean potential temperature contour intervals are 20 and 2 K, respectively, with a few contour values indicated for reference. The zero (bold), eastward (thin solid), and westward (thin dashed) flow lines have contours every 4 m s^{-1} in the atmosphere and every 5 cm s^{-1} in the ocean. Only the top 2 km of the 5.2-km ocean are shown. The presence (and its extent) or absence of ice is noted in the space between the atmosphere and ocean panels.

polar latitudes depends on the presence or absence of ice. Aqua has ice over both poles and Drake has ice only over the South Pole. In those climates and/or hemispheres without ice (Ridge, EqPas, and the Northern Hemisphere of Drake) there are polar easterlies that disappear when ice is present—see Figs. 4d, 4a, 4b, and 4e, which plot the zonal-mean surface wind stress, the surface air temperature, and the fractional ice cover, respectively.

Figure 5 (top panels) shows the (Eulerian mean) atmospheric meridional overturning circulation in our coupled climates. In all cases we observe mean Hadley cells symmetrically disposed about the equator (over the seasonal cycle the upwelling branch "follows the sun," migrating back and forth across the equator) and Ferrel cells in middle latitudes with an obvious connection to ageostrophic motion associated with the
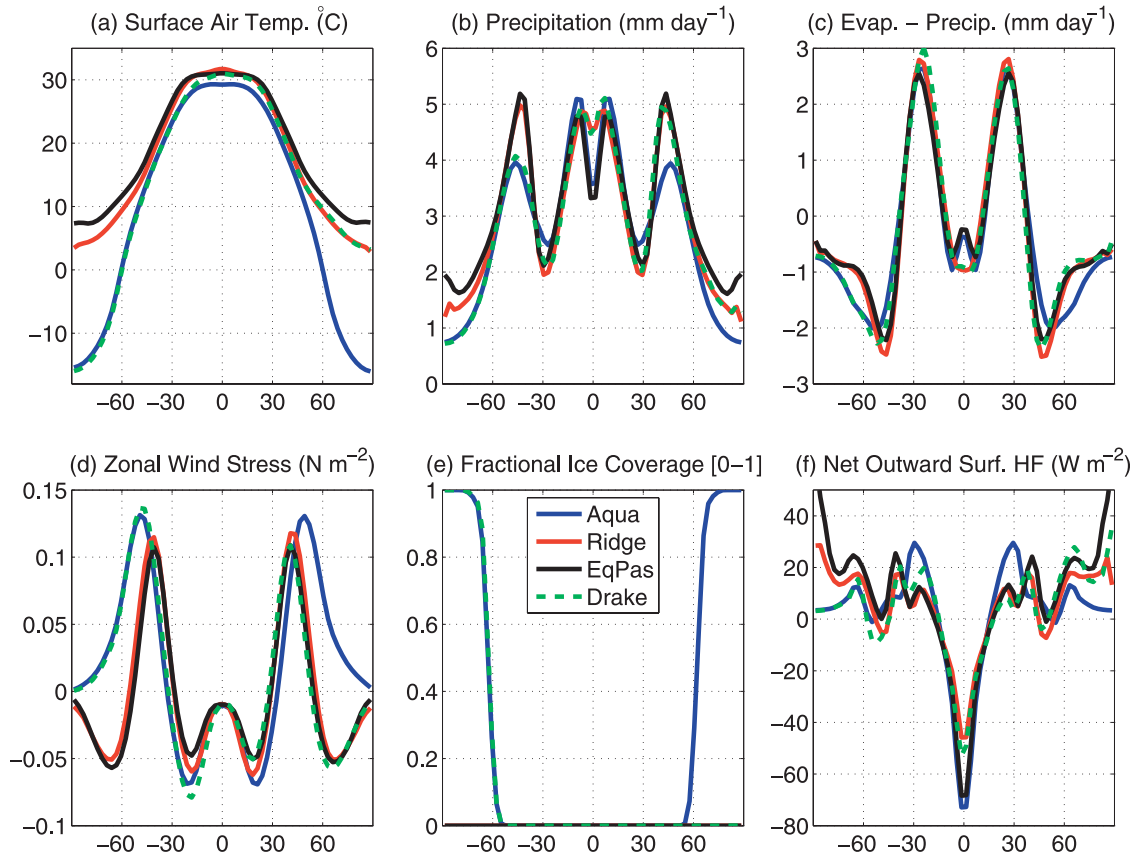
FIG. 4. Twenty-year time and zonal average surface fields: (a) surface air temperature (°C), (b) precipitation (mm day^{-1}), (c) evaporation minus precipitation (mm day^{-1}), (d) zonal average wind stress (N m^{-2}), (e) fractional ice coverage (0–1), and (f) net outward surface heat flux (W m^{-2}).

surface wind stress patterns seen in Fig. 4d. In those climates in which there are polar easterlies (Ridge, EqPas, and the Northern Hemisphere of Drake) we also observe an associated (weak) overturning circulation at high latitudes. The Hadley cells are about 20% weaker relative to earth observations.

Figure 6 shows the moisture and salinity distributions of the various climates. The specific humidity in all climates is largest at low levels in the tropics and diminishes with increasing height and latitude, reflecting the sensitive dependence of the saturated vapor pressure of water on temperature. The warm climates of Ridge and EqPas have considerably elevated values of specific humidity relative to cold climates. The air is very dry over the frozen poles of the Aqua climate and the frozen south pole of Drake. As discussed in more detail below, excess of evaporation over precipitation in the middle latitudes of all climates (see Fig. 4c) results in the establishment of middle-latitude salt lenses in the ocean, with fresher water found at the surface in the tropics and, especially in association with ice, over the poles.

The same general structure of H_A is seen in all four coupled calculations (see Ridge and Drake examples in Fig. 7). There is around 1 PW of latent heat transport equatorward at ±10° and 4 PW poleward at ±38°. Dry static energy is transported poleward at all latitudes, peaking in the topics and middle latitudes. At 50° we note that the meridional energy transport is roughly equally partitioned between dry static energy and latent heat flux. This is in accord with the reference calculation of an idealized suite of atmospheric calculations presented in O'Gorman and Schneider (2008). Comparing Fig. 7 with the data presented in Pierrehumbert (2002), our coupled model, despite its highly idealized configuration, broadly captures the observed meridional distribution of latent heat flux, but with a more pronounced double peak in the dry static energy flux.

Figures 7b and 7d show that the major part of the poleward energy transport is achieved by transient eddies, with the mean circulation playing a considerably smaller role, even at low latitudes. Of course the atmospheric standing eddy contribution in all of our calculations is by construction very small (there is no orographic
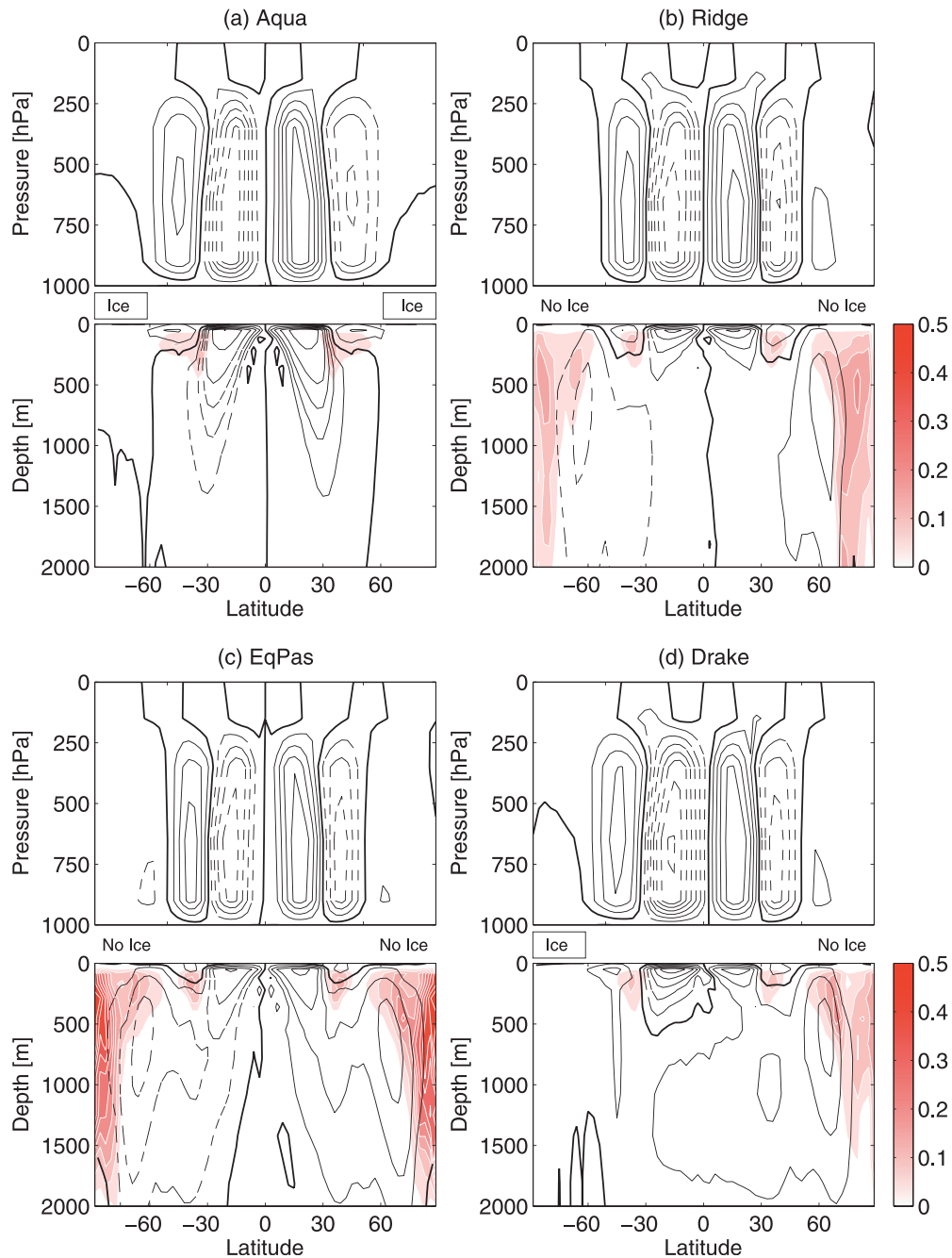
FIG. 5. Twenty-year time and zonal average meridional overturning circulation in the atmosphere (Eulerian mean) and ocean (residual mean). The zero (bold), clockwise (thin solid), and counterclockwise (thin dashed) overturning contours are every 10 Sv $= 10^{10}$ kg s^{-1} in both fluids. The zonal mean convective index in the ocean is also shown (shaded red and contoured every 0.05).

forcing). In Drake, where there is significantly less poleward H_O in the Southern Hemisphere relative to Ridge but enhanced H_T (see discussion below), this difference is largely accounted for by enhanced transport of dry static energy in transient eddies.

Although there is broad similarity in patterns of circulation between the atmospheres of our coupled calculations, the ocean circulations in the various basin geometries are markedly different from one another, as we now go on to discuss.
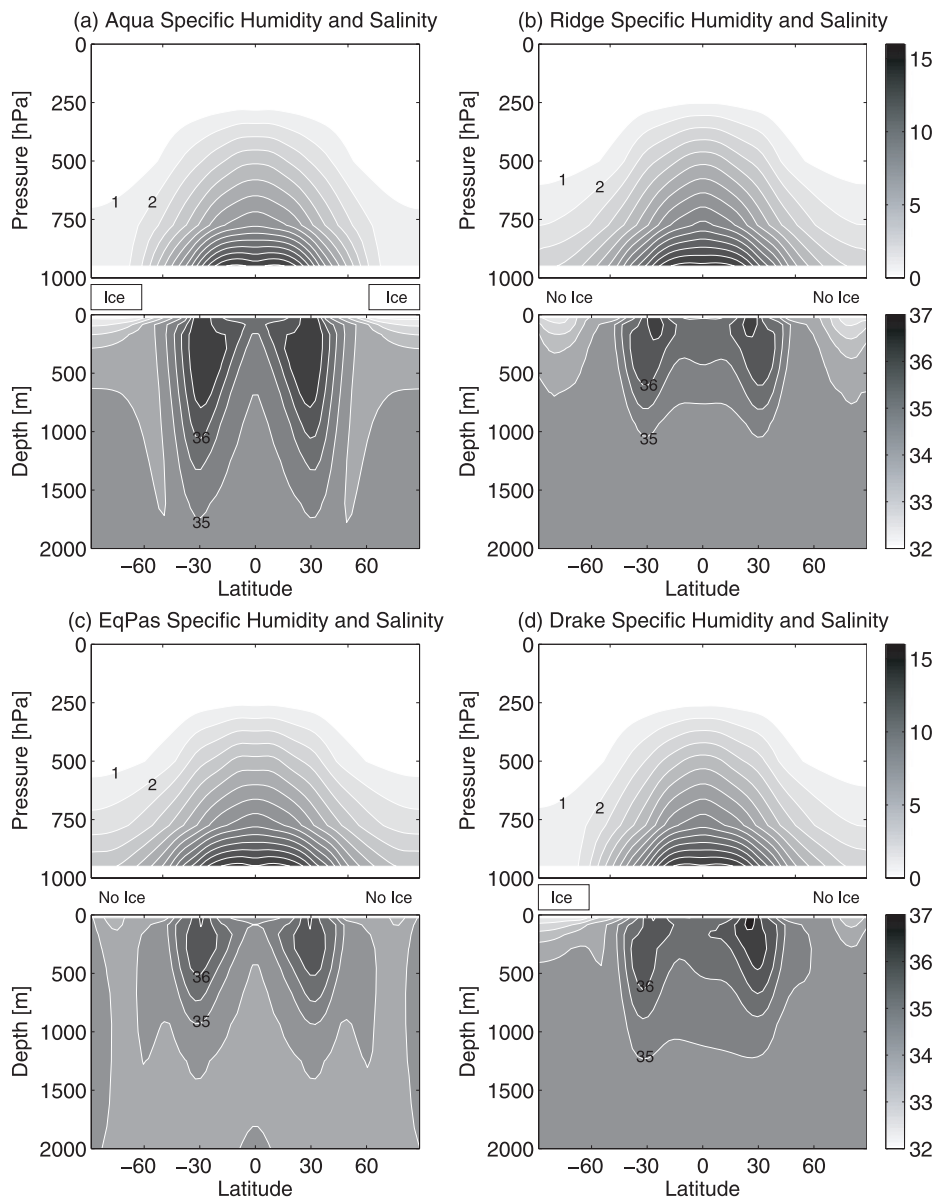
FIG. 6. Twenty-year time and zonal average atmospheric specific humidity (contours every g kg^{-1}) and oceanic salinity (contours every 0.5 psu). Only the top 2 km of the 5.2-km ocean are shown. The presence (and its extent) or absence of ice is noted in the space between the atmosphere and ocean panels.

1) AQUA

As discussed in detail in Marshall et al. (2007),[2] in the absence of any meridional barriers, there is no possi-

---

[2] There are some differences in model parameters between the Aqua simulation presented here and that described in Marshall et al. (2007). In this study we use more typical values of snow and ice albedos (cold/warm snow albedo: 0.80/0.45; ice albedo: 0.60) and an ocean surface albedo that increases with zenith angle (as in Briegleb et al. 1986). While the broad climatologies of the Aqua simulation described here and in Marshall et al. (2007) are very similar, the solution presented here has somewhat less ice cover.

bility of Sverdrup balance in the Aqua ocean. Flow is predominantly zonal and reflects the sense of the surface winds driving them: there is westward flow in the tropics and eastward flow in middle latitudes. Ekman pumping centered on ±30° and upwelling in a rather narrow band along the equator leads to Eulerian mean overturning cells that extend down to the bottom of the ocean basins. There is a compensating eddy-driven circulation. The resulting "residual" overturning (discussed at length in Marshall et al. 2007) features strong subtropical cells (STCs) with a strength of some 60 Sv (Sv ≡ 10^6 m^3 s^{-1}) (Fig. 5, top left). It is tempting to call
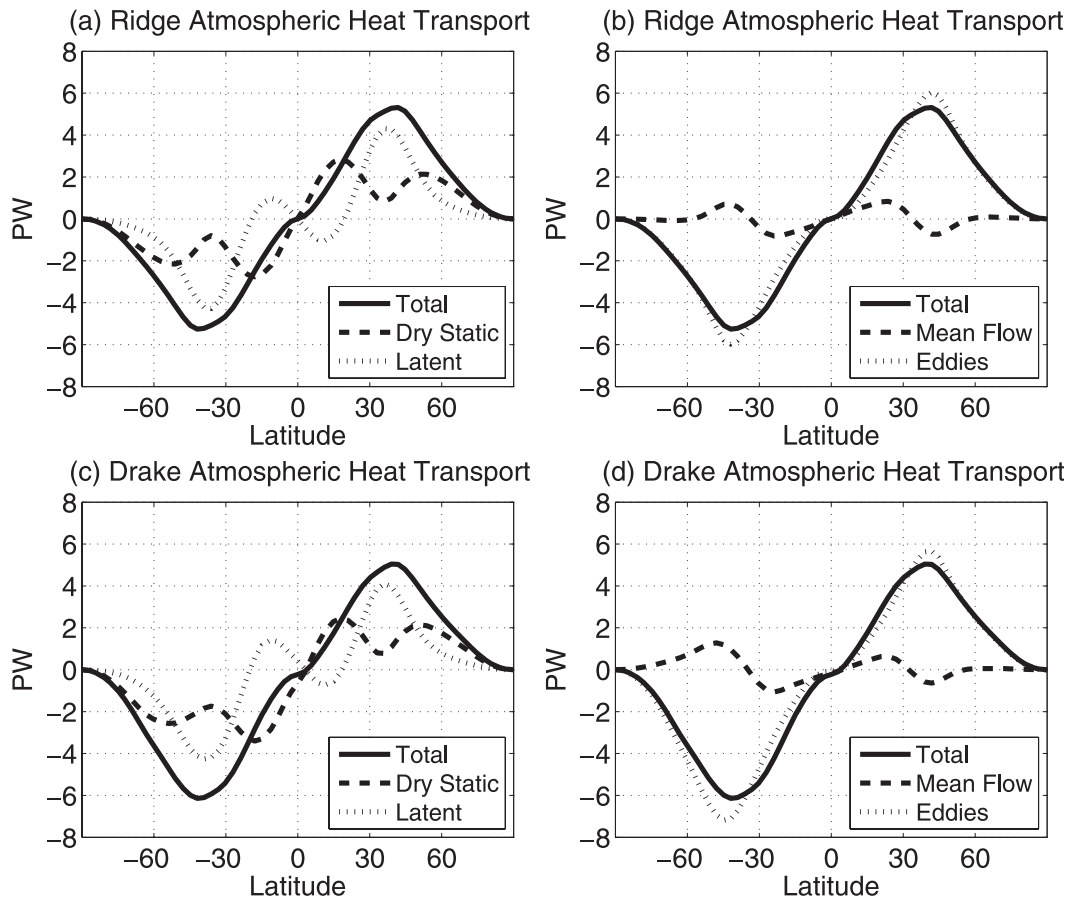
FIG. 7. Atmospheric heat transport (in PW) for Ridge (top) and Drake (bottom) decomposed into (left) dry static and latent components and (right) mean flow and transient eddy components.

them the ocean's Hadley cells, although they are mechanically rather than thermally forced. Associated with this overturning circulation, the thermocline features two "lenses" of warm, salty fluid overlying much colder, fresher water. In middle and high latitudes, Ekman transport is almost entirely compensated by eddy-induced circulation resulting in near-zero residual transport, in direct analogy to the vanishing of the Deacon cell in the present climate.

Mechanisms of H_O in the various configurations are revealed in Fig. 8. In Aqua, H_O is dominated by Eulerian mean (Ekman driven) overturning in the tropics, which is partially offset by heat transport due to eddy-induced circulation—see Fig. 8a. In middle and high latitudes the Eulerian mean and eddy-induced contributions largely offset one another, leading to weak residual overturning circulation and rather small heat transports north of 50°: H_O reaches a maximum of 2.4 PW at ±15°, dropping to less than 0.35 PW poleward of ±50°, and H_T reaches a peak of 6.5 PW at ±36°. Ice caps extend down to ~61° in both hemi-

spheres of Aqua and surface air temperatures drop to below −15°C at the poles and peak at 28°C in the tropics (see Fig. 4a).

2) RIDGE

The ocean circulation in Ridge is quite different from that of Aqua. In particular, there are no ice caps owing to enhanced heat transport by the ocean facilitated by the presence of a meridional barrier and hence western boundary currents. The barrier interrupts zonal flow and induces Sverdrupian gyral circulation (Fig. 9), the sense of which reflects the (westward) integrated "curl" of the driving wind stress. These wind-driven gyres are confined to the thermocline, the upper 1000 m or so of the ocean. The subtropical and subpolar gyres reach magnitudes of 100 Sv while the equatorial and polar gyres have a strengths of 20 and 25 Sv, respectively. The streamfunction for the depth-integrated flow (≡ barotropic streamfunction) is shown in Fig. 9 and is directly related to the pattern of surface wind stress, which (see Fig. 4d), through the Sverdrup relation,
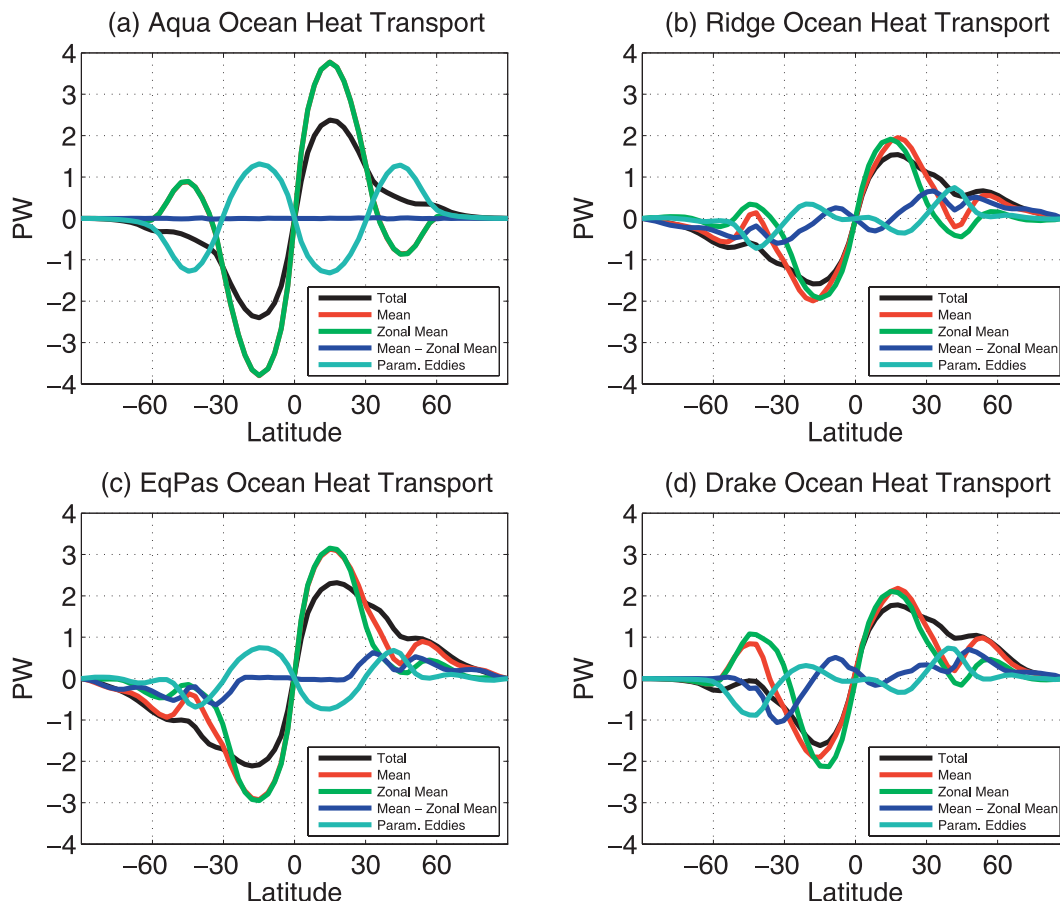
FIG. 8. Ocean heat transport (PW) for (a) Aqua (b) Ridge, (c) EqPas, and (d) Drake decomposed into total, mean flow ($\overline{vT}^t$), zonal mean flow ($\bar{v}^{xt}\overline{T}^{xt}$), mean flow − zonal mean flow (horizontal circulations), and parameterized eddies.

explains the subtropical and subpolar gyres as well as the equatorial gyres feeding a countercurrent (i.e., directed in the opposite sense to the local winds) along the equator and anticyclonic polar gyres.

The meridional overturning circulation again yields STCs (see Fig. 5, top right) but, because a zonal pressure gradient now exists, partly balancing the zonal wind stress, they are of diminished strength (only 43 Sv in Ridge compared to 60 Sv in Aqua) and are much shallower. The ridge also supports deep meridional overturning circulation (MOC) emanating from the poles and upwelling in the middle latitudes. The ocean convective index, shaded red in Fig. 5, reveals that deep polar convection is present in Ridge but absent in Aqua and clearly indicates an association between the high-latitude MOC and polar convection. Polar convection is driven by the disequilibration between the sea surface temperature and the surface air temperature, facilitated by meridional advection of energy in boundary currents, which results in enhanced air–

sea flux in the presence of a high-latitude ridge (see Fig. 4f).

Owing to weaker subtropical cells and an equatorial gyre transporting energy equatorward, H_O is much smaller in Ridge (1.5 PW at $\pm18°$) than Aqua in the tropics—see Figs. 8a,b. In middle and high latitudes, however, H_O in Ridge exceeds that in Aqua due to the presence of subtropical and subpolar gyres, which both act to transport heat poleward. This mechanism of meridional heat transport by gyres can be visualized by inspection of Fig. 9, which overlays departures in sea surface temperature from its zonal average on the barotropic streamfunction. The role of the gyres (absent in Aqua) can also be seen in the difference between the contributions to the heat transport by the mean and zonal mean circulations seen in Fig. 8b. Here H_O is directed poleward and remains substantial in both the subtropical and subpolar gyres, exceeding 0.5 PW all the way up to $\pm70°$, and H_T peaks at 6.0 PW at $\pm36°$. As mentioned previously, there is no ice present in Ridge.
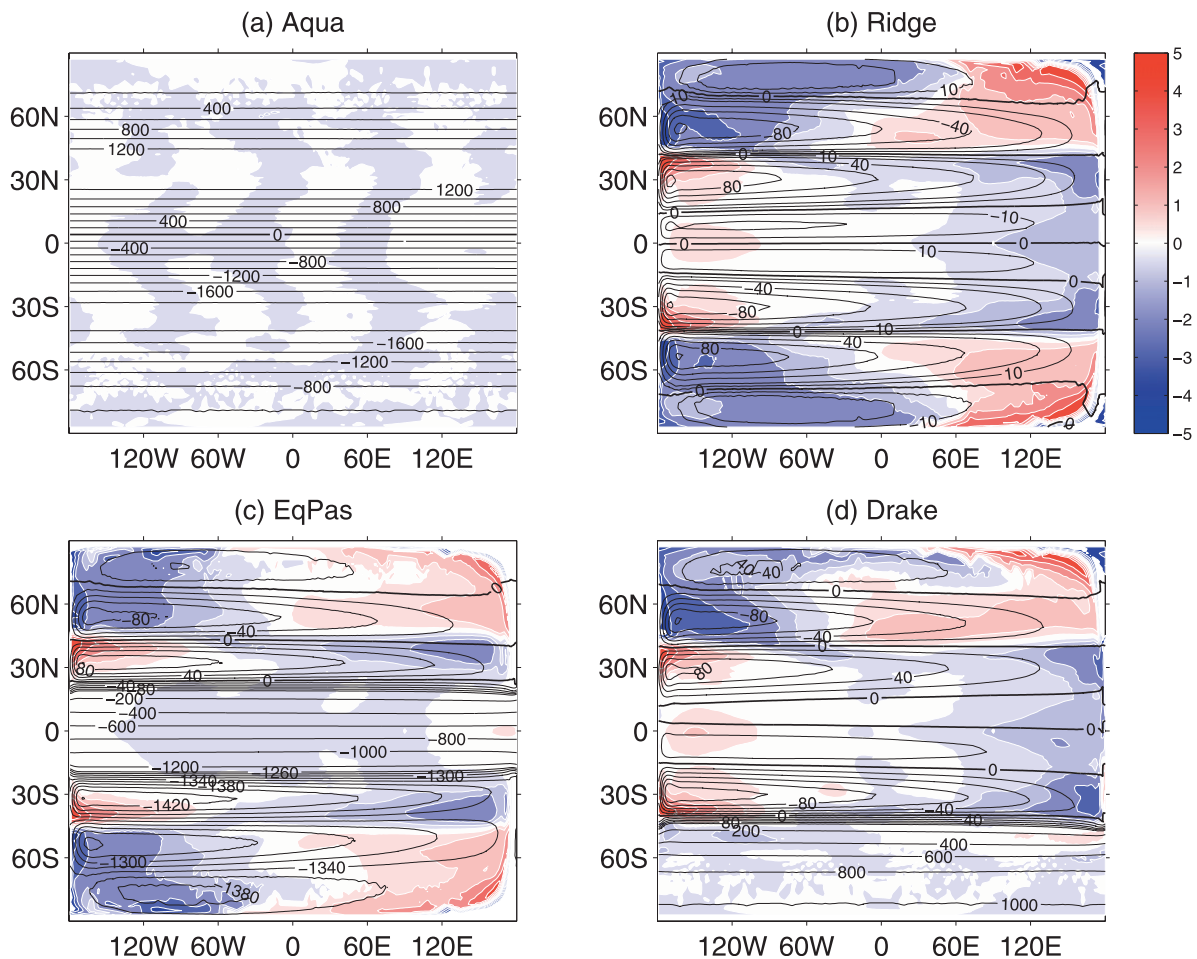
FIG. 9. Oceanic depth integrated flow (Sv; black contour lines) overlying SST deviation from its zonal average ($\overline{SST}^t - \overline{SST}^{xt}$;°C; blue–red shading). Note that the contour interval for the depth-integrated flow changes from 20 Sv in regions of gyral flow to 200 Sv in regions of zonal flow. An extra contour at 10 Sv is included in *Ridge* to help identify the equatorial gyres feeding a countercurrent along the equator.

Surface air temperatures rise to 32°C in the tropics and fall to 3°C at the poles (see Fig. 4a).

3) EQPAS

The removal of the meridional barrier between 20°S and 20°N in EqPas results in a major change in tropical ocean dynamics relative to that found in Ridge. The gap permits strong zonal ocean flow in the tropics, peaking at 90 cm s^{-1} along the equator with a total volume transport of 1300 Sv through the equatorial passage (Figs. 3 and 9). The absence of a zonal pressure gradient along the equator has two important consequences: First, equatorial gyres and their associated equatorward heat transport are no longer present. Second, the subtropical cells (see Fig. 5) are of the same magnitude as in Ridge (43 Sv), despite a wind stress which is about 20% weaker at 15° (Fig. 4d). Equatorial upwelling also draws

water up from the abyss, which originates from high latitudes sustaining two deep overturning cells, one in each hemisphere. They have strength on the order of 35 Sv, with 20 Sv upwelling in the tropics. This should be contrasted with the deep overturning cells found in Ridge, which are weaker and confined to high/middle latitudes.

The combined effect of the absence of equatorial gyres and the presence of deep meridional overturning circulations extending from pole to equator is to enhance H_O at all latitudes in EqPas relative to Ridge (see Figs. 8b,c); H_O in EqPas reaches a peak of 2.2 PW at $\pm 18°$, exceeding that in Ridge by 0.5 PW up to a latitude of $\pm 45°$. As in Ridge, there is no ice. As discussed in detail in section 3, the H_T in EqPas, however, is virtually identical to that of Ridge at all latitudes (see Fig. 10). Surface air temperatures reach 31°C in the tropics and
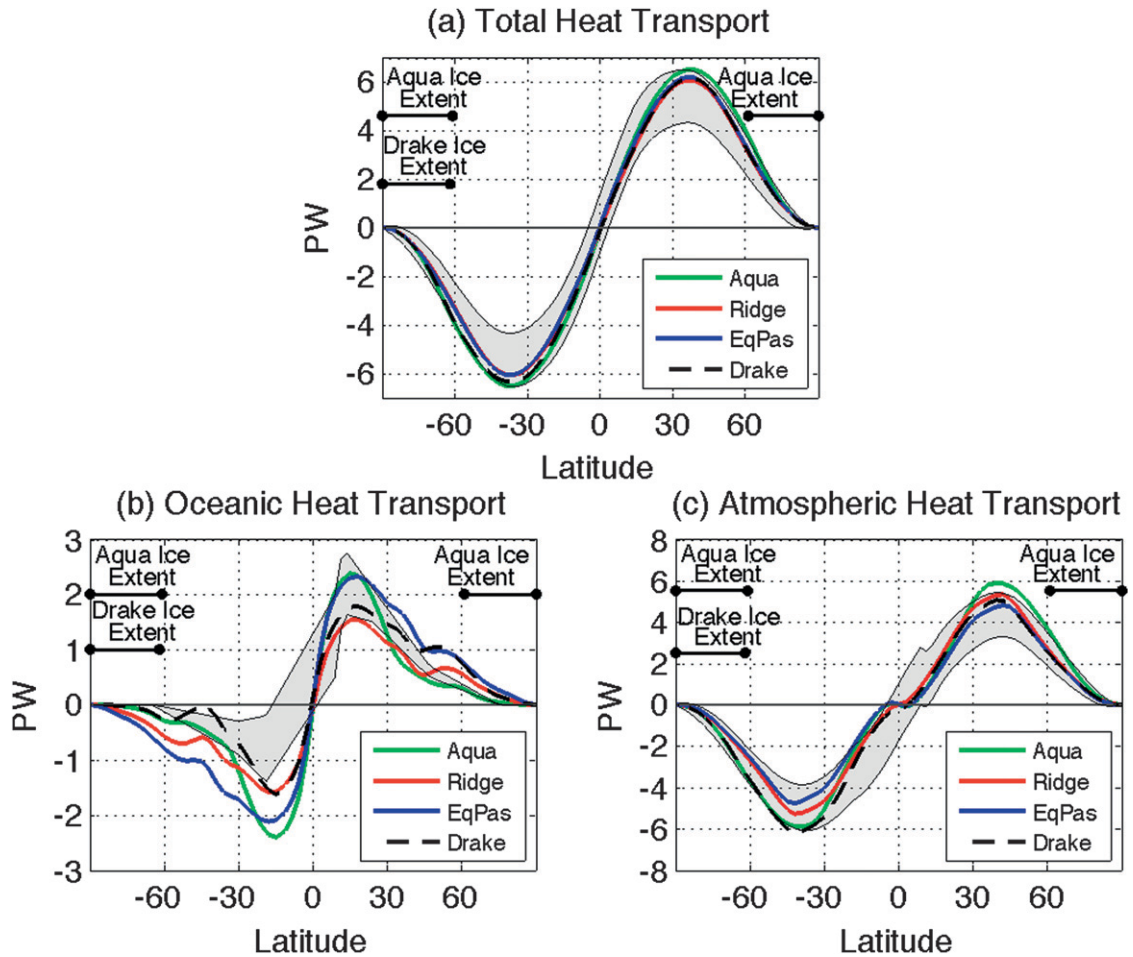
FIG. 10. (a) Total, (b) oceanic, and (c) atmospheric heat transport for the aquaplanet configurations shown in Fig. 2. Uncertainty envelopes for observation-based estimates of Earth's heat transport are shown by the shaded regions (taken from W05).

remain a balmy 8°C at the poles. Interestingly, air temperatures at polar latitudes in EqPas are some 5°C warmer than those found in Ridge, a consequence, one might suppose, of enhanced meridional ocean heat transport.

4) DRAKE

With a meridional barrier everywhere except south of 40°S, Drake is similar to Aqua in the high-latitude Southern Hemisphere and to Ridge in the Northern Hemisphere. Of greatest significance is that the gap south of 40° permits zonal flows that inhibit H_O: the weak residual meridional overturning circulation results in a H_O that is much reduced relative to that found in Ridge and EqPas. In this manner the South Pole becomes "isolated" from warm waters in the tropics and ice forms extending from the South Pole to ~62°S, much as found in Aqua. South of 40°S there is a strong

eastward-flowing ocean current with a peak of 25 cm s^{-1} at 48°S (see Fig. 3), analogous to the Antarctic Circumpolar Current of our modern climate. The Northern Hemisphere, however, remains ice free in the presence of a ridge. A feature unique to Drake is a cross-equatorial deep meridional overturning circulation. Sinking occurs in the polar region of the Northern Hemisphere (see Fig. 6) with roughly 12 Sv crossing the equator and 8 Sv upwelling in the Southern Hemisphere where the meridional gap is absent. This interhemispheric asymmetry is vividly evident in the hydrological fields (specific humidity and salinity) presented in Fig. 6, where we observe a pronounced freshening of the surface waters over the South Pole relative to the North Pole. This suppresses the tendency for deep ocean convection in the south while enhancing it in the Northern Hemisphere, the positive feedback discussed in Toggweiler and Bjornsson (2000) and references therein.

In the Northern Hemisphere, H_O peaks at 1.8 PW at 18°N and exceeds 0.75 PW all the way up to 60°N (see Figs. 8 and 10). In the Southern Hemisphere, poleward H_O peaks at 1.6 PW at 15°S and is quite small outside of the tropics. In the Northern Hemisphere, the poleward H_T is nearly identical to that found in Ridge and EqPas, peaking at 6.1 PW at 36°N. In the Southern Hemisphere H_T peaks at 6.4 PW at 36°S, compared to the 6.5 PW found in Aqua. Surface air temperatures reach 31°C in the tropics and are −16°C at the South Pole and 3°C at the North Pole (Fig. 4a).

In summary, we see that geometrical constraints on ocean heat transport have a profound effect on the climate of our aquaplanet simulations. Having discussed the nature of the circulations in these coupled solutions, we now go on to discuss their controls on meridional energy transports.

3. Total heat transport

Figure 10 is a plot of the total heat transport and its partition between the atmosphere and ocean in the coupled calculations just described. We see that, even though the diverse ocean circulations yield a range of H_O varying by up to a factor of 2, the meridional distributions of atmosphere plus ocean heat transport, H_T, varies much less between the solutions and, in those climates in which there is no ice, are almost identical. This is particularly striking when one compares Ridge, EqPas, and the Northern Hemisphere of Drake: H_O varies substantially among these solutions whereas H_T does not. The difference in H_T between Aqua, the Southern Hemisphere of Drake, and Ridge is a consequence of the presence of large ice sheets in the former two solutions. As will be discussed below, due to enhanced reflected solar radiation at high latitudes in Aqua and the Southern Hemisphere of Drake, there is an augmented gradient in absorbed incoming energy between the equator and poles, resulting in a higher H_T relative to Ridge. Nevertheless, despite the marked interhemispheric difference in ice cover in Drake, H_T remains nearly antisymmetric about the equator: poleward H_T is greater in the south relative to the north by ~0.3 PW (with < 0.1 PW crossing the equator). These results are now explored using the Legendre polynomial expansion model presented in S78. An instructive two-box model, which may have additional physical appeal, is also of interest and is described in the appendix.

S78 argued that H_T was largely independent of the details of the mechanisms of atmospheric and oceanic heat transport processes and should depend primarily on solar forcing, planetary albedo, and astronomical parameters. Stone's result is often interpreted as being a consequence of the atmosphere being close to a state in which the outgoing longwave radiation is uniform in latitude due to the efficient meridional energy transport by the atmosphere (see, for example, the discussion in Frierson et al. 2007). However, in Stone's detailed calculations (his section 3), rather than assuming an absence of OLR gradients, he notes a serendipitous cancellation of the effects of the gradients in OLR with gradients in absorbed solar radiation associated with interhemispheric variations in albedo. Moreover, in the present aquaplanet calculations in which ocean circulation plays an important role in setting ice extent and in which ocean circulation depends on forcing from the overlying atmosphere, the planetary albedo and gradients in albedo cannot be assumed to be fixed a priori. For these reasons we employ the framework introduced by S78 to help us understand the controls on meridional energy transport. We go on to reexamine total heat transport of the present climate using ERBE data.

a. Formulation of the Stone (1978) model

We first briefly review the series representation of the heat transport following Stone [(1978), Eqs. (6)–(18) on 127–132]. Assuming a steady state, the balance between absorbed radiation, outgoing radiation, and total heat transport is defined as

$$\frac{dH_T}{d\phi} = 2\pi R^2 \cos\phi[S(\phi)a(\phi) - I(\phi)], \qquad (1)$$

where ϕ is latitude, R is the radius of the earth, S the incoming top of the atmosphere (TOA) solar radiation (W m^{-2}), a the coalbedo (1 − albedo: the fraction of solar radiation absorbed), and I is the TOA outgoing longwave radiation (W m^{-2}).

Employing the nondimensionalization of S78, we define

$$x = \sin\phi, \qquad (2)$$

$$S = \frac{S_0}{4}s(x), \qquad (3)$$

$$I = \frac{S_0}{4}i(x), \qquad (4)$$

and

$$H_T = \frac{\pi R^2 S_0}{2}f(x) \qquad (5)$$

and rewrite Eq. (1) as

$$\frac{df}{dx} = s(x)a(x) - i(x), \qquad (6)$$

where $s(x)$, $i(x)$, and $f(x)$ are nondimensionalized versions of S, I, and H_T, respectively.

By expanding data from Ellis and Vonder Haar (1976) for s, a, and i in a series of even-order Legendre polynomials, S78 finds that the first two terms of each expansion capture most of the structure in the fields. That is,

$$s(x) \approx s_0 P_0(x) + s_2 P_2(x), \qquad (7)$$

$$a(x) \approx a_0 P_0(x) + a_2 P_2(x), \qquad (8)$$

and

$$i(x) \approx i_0 P_0(x) + i_2 P_2(x), \qquad (9)$$

where

$$P_0(x) = 1, \quad P_2(x) = \frac{1}{2}(3x^2 - 1). \qquad (10)$$

Figure 11 shows nondimensionalized Aqua, Ridge, and Drake planetary coalbedo a and OLR i from our Aqua, Ridge, and Drake simulations expanded in zeroth- and second-order Legendre polynomials. Incoming solar radiation s is represented extremely well by the zeroth- and second-order terms and is not shown.

Respectively, s_0, a_0, and i_0 are the mean incoming solar radiation [normalized to 1 by Eq. (3)], coalbedo, and OLR. Assuming the system is in equilibrium, OLR must balance absorbed incoming solar radiation:

$$i_0 = s_0 a_0. \qquad (11)$$

The second-order coefficients, s_2, a_2, and i_2, are a measure of the equator–pole gradients in these fields. Note that s_2 (as well as s_0) is defined externally of the climate system. The coefficients of i and a will be dependent, at least to some degree, on atmospheric and oceanic dynamics. In particular, if the system were extremely efficient at transporting energy, then i_2 would approach zero and the energy reradiated to space would be uniformly distributed in latitude. The mean coalbedo a_0 [and hence i_0 by Eq. (11)] can be sensitive to climate dynamics to the extent that dynamics affect ice extent, cloud cover, and/or land albedo.

Using these truncated expansions and integrating Eq. (6) yields

$$f \approx \left(s_0 a_0 + \frac{1}{5}s_2 a_2 - i_0\right)(x - 1)$$
$$+ \left(s_2 a_0 + s_0 a_2 + \frac{2}{7}s_2 a_2 - i_2\right)\frac{(x^3 - x)}{2}. \qquad (12)$$

On evaluating the coefficients, the $(x - 1)$ term is found to be negligible compared to the $(x^3 - x)$ term, as one would expect since there is little to no total heat transport across the equator ($x = 0$), leaving

$$f \approx -\left(s_2 a_0 + s_0 a_2 + \frac{2}{7}s_2 a_2 - i_2\right)$$
$$\times \frac{(x - x^3)}{2} \quad \text{(four-term } H_T \text{ balance)}. \qquad (13)$$

Note that the last three terms in Eq. (13) include second-order coefficients that are expected to be the most sensitive to atmosphere and ocean dynamics.

Remarkably, when S78 estimated the magnitude of the terms in Eq. (13) using data, he found that $s_0 a_0 + (2/7)s_2 a_2 - i_2 \approx 0$ (attributed to the correlation between local absorption of shortwave radiation and local emission of longwave radiation; $s_0 a_2 \approx i_2$); see Table 1. Thus, as an approximation for H_T, S78 arrived at

$$f \approx -(s_2 a_0)\frac{(x - x^3)}{2} \quad \text{(one-term } H_T \text{ balance)}. \qquad (14)$$

For the remainder of this paper, Eqs. (14) and (13) will be referred to as the one- and four-term balances, respectively. It is worth reemphasizing that Eq. (13) should not be interpreted as suggesting that f (and hence H_T) is a consequence of terms on the rhs. In actuality, i_2 is a consequence of H_T rather than vice versa.

The one-term balance has at least two noteworthy characteristics:

(i) Coefficients a_2 and i_2, which are the most likely to depend on the details of atmospheric and oceanic dynamics, do not appear. Hence, at this level of approximation, H_T is insensitive to particular atmospheric and oceanic circulations (except as they influence the mean planetary coalbedo a_0). This implies that ocean heat transport differences between two different climates would be compensated by equal and opposite changes in atmospheric transport.

(ii) The one-term balance predicts a decrease in H_T if the mean planetary coalbedo (albedo) decreases (increases). If this decrease in planetary coalbedo were spatially uniform, the absorbed solar flux would decrease everywhere without altering the differential heating responsible for driving meridional heat transport. Changes in albedo, however, are typically nonuniform and, for example, are
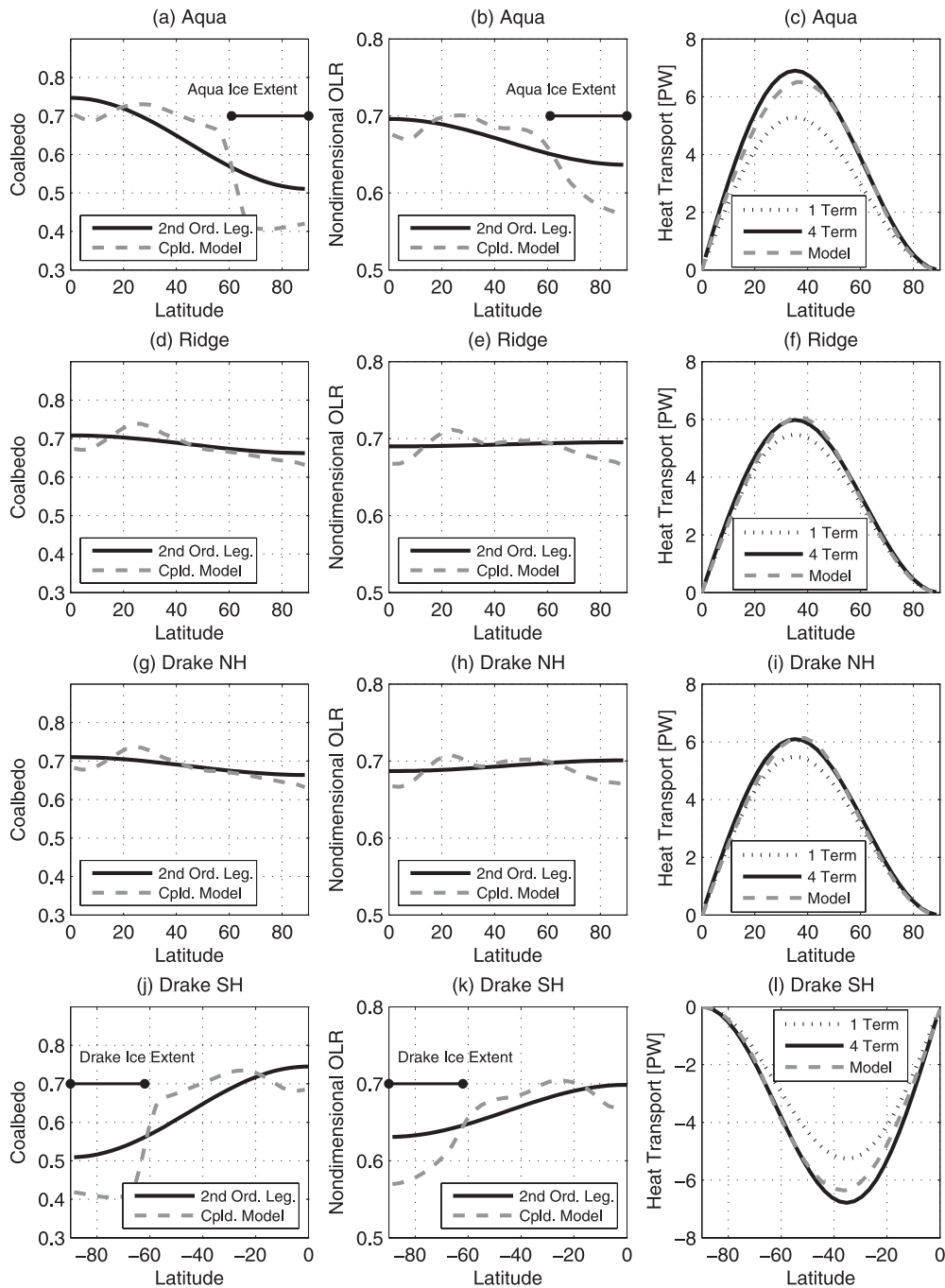
FIG. 11. (left) Coalbedo and (middle) nondimensionalized OLR, expanded in zeroth- and second-order Legendre polynomials (denoted "2nd Ord. Leg.") for (first row) Aqua, (second row) Ridge, (third row) Northern Hemisphere (NH) Drake, and (fourth row) Southern Hemisphere (SH) Drake; (right) coupled model total heat transport (dashed) and its one-term (dotted) and four-term (solid) balances.

likely to involve growth or retreat of polar ice. This suggests that other terms, such as those containing a_2, the equator–pole gradient in coalbedo, may be important in Eq. (13). This is, indeed, the case in our coupled climate model, as discussed below.

Given the implications of point (i) and the consequence highlighted in point (ii), the efficacy of the one-term and four-term balances are now tested using our coupled model results as well as the ERBE dataset (http://iridl.ldeo.columbia.edu/SOURCES/.ERBE/).

TABLE 1. Terms used in the S78 total heat transport expansion, Eq. (13). The first column gives the (nondimensional) one-term balance whereas the Sum column (the sum of the four terms) gives the four-term balance. The last three columns tabulate estimates of total heat transport (f dimensionalized back to H_T in PW) from one- and four-term balances together with the total heat transport found in the coupled model (last column).

	$-s_2 a_0$	$-s_0 a_2$	$-\frac{2}{7} s_2 a_2$	$+i_2$	Sum	Max H_T one-term	Max H_T four-term	Max H_T realized
Aqua NH	0.315	0.158	−0.021	−0.040	0.412	5.28	6.90	6.51
Ridge NH	0.327	0.031	−0.004	0.004	0.357	5.47	5.98	6.07
Drake NH	0.328	0.031	−0.004	0.009	0.364	5.49	6.09	6.14
Drake SH	0.314	0.157	−0.021	−0.045	0.405	5.26	6.79	6.36
NH (Stone)	0.319	0.192	−0.026	−0.165	0.320	5.35	5.36	5.85
SH (Stone)	0.319	0.217	−0.029	−0.179	0.328	5.35	5.50	5.69
NH (ERBE)	0.326	0.199	−0.027	−0.133	0.365	5.46	6.12	5.85
SH (ERBE)	0.322	0.262	−0.035	−0.183	0.365	5.40	6.12	5.69

b. Application to the aquaplanet solutions

The total heat transport from the coupled model runs is now compared with the one- and four-term balances. The coupled model coalbedo and nondimensional OLR are expanded in zero- and second-order Legendre polynomials, as shown in Fig. 11. For Aqua, the first two terms of the expansion capture the gross equator to pole difference in a and i. There are, however, large differences between the coupled model fields and these low-order fits, particularly with respect to their inability to capture the sharp changes in coalbedo and OLR across the ice edge at ~61°. Despite this, the four-term balance does reasonably well at reconstructing H_T. In contrast, the one-term balance does not adequately capture H_T when large ice caps are present.

There is a much smaller difference between the one- and four-term balances for the Ridge and EqPas solutions, as can be seen in Fig. 11. (These two climates have virtually identical distributions of albedo, OLR, and H_T; only those for Ridge are shown). Ridge has much more absorption of shortwave radiation at high latitudes due to the absence of ice and hence a relatively flat profile of albedo. Similarly, the OLR profile does not have much structure. Since a and i depend little on latitude (a_2 and i_2 are close to zero), it is not surprising that there are much smaller differences between the one- and four-term balances. The four-term balance also captures H_T well, whereas the one-term balance underestimates H_T by about 0.75 PW. The results for the Drake are very similar to Ridge in the Northern Hemisphere and to Aqua in the Southern Hemisphere.

In summary, S78's one-term balance, from which his major summary conclusions flow, does a rather poor job at representing H_T across our suite of aquaplanet climates. This is not because there are significant gradients in OLR, but rather because of the presence of gradients in albedo associated with ice extent. Thus, for example,

in Table 1 the one-term balance (first column) predicts that H_T increases on moving from Aqua to Ridge, whereas the four-term balance (last column) correctly predicts that H_T significantly decreases because of the absence of interhemispheric albedo effects (captured by the $s_0 a_2$ terms in the second column). Stated again, even though the planetary albedo increases in the presence of polar ice, tending to decrease H_T, enhanced gradients in albedo more than offset this tendency. Thus, we see that Stone's one-term balance fails, not because of gradients in OLR (which are small in all of our aquaplanet climates; see middle panel of Fig. 11) but because of enhanced gradients in albedo between equator and pole.

c. Application to ERBE data

Top-of-atmosphere measurements of incoming and outgoing radiation gathered during ERBE (Barkstrom et al. 1989; Bess and Smith 1993) have been used by various authors to estimate H_T. The general procedure is to set $H_T = 0$ at one of the poles and integrate Eq. (1) from that pole to the other. However, the data must be balanced a priori to avoid an accumulation of errors, which can lead to a large residual heat transport at one pole or the other (Carissimo et al. 1985; W05). One such method is to simply remove the mean net TOA flux evenly over the entire globe, which yields a maximum poleward heat transport of about 5.8 PW (see Fig. 12). Using slightly more sophisticated balancing techniques, estimates of peak H_T have settled around 5.5 PW (Carissimo et al. 1985; TC01). Using the S78 one-term balance of H_T as a constraint, rather than ad hoc balancing, W05 obtains a profile similar to that of TC01. Carissimo et al. (1985) ascribes an error of ±1 PW to H_T estimates, similar to that generated by the approach of W05. Keith (1995) estimates an uncertainty of ±0.5 PW. The studies of Keith (1995), TC01, and W05 all use ERBE data.
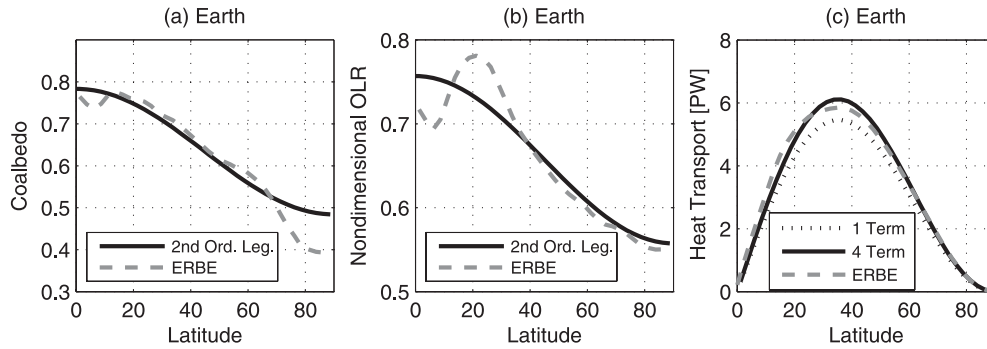
FIG. 12. As in Fig. 11 but using Northern Hemisphere ERBE data. Prior to computation of the total heat transport, the ERBE data were adjusted by subtracting the mean imbalance from the net TOA radiation.

Figure 12 repeats the S78 calculation using ERBE data. We expand a and i in Legendre polynomials, as shown in the left and middle panels of Fig. 12. While much of the structure is indeed captured by the first two terms in the expansion, the higher-order terms (especially for i) cannot be neglected. For example, the relatively low OLR due to the presence of clouds in the intertropical convergence zone is not captured. When these coefficients are used to evaluate Eq. (13), the difference between the one-term and four-term balance is now ~15%, whereas with the data employed by S78 it was ~0% (see Table 1). In the present calculation using ERBE data, the one- and four-term balances differ by about 0.75 PW near 35°N, a considerable magnitude.

Figure 12 presents our estimate of H_T based on ERBE observations: the data were first balanced by subtracting the mean residual from the net TOA radiation and integrated meridionally from one of the poles, yielding a maximum of 5.8 PW. Also plotted in Fig. 12 is the four-term balance, which clearly more closely follows the H_T curve than does the one-term balance. It should be noted, however, that the one-term balance is a closer match to results based on more involved H_T estimation methods that put the peak value at 5.5 PW (TC01; W05). In the case of W05, this is possibly a result of having used the S78 one-term balance as a prior assumption in the calculation of H_T. In the study of TC01, this result is less clear because the exact details of the TOA radiation adjustments are not given.

4. Discussion and conclusions

We have described a series of experiments on an aquaplanet in which geometrical constraints on ocean circulation, induced by the presence or absence of meridional barriers, result in starkly different climate states. The reference solution without barriers maintains ice over both poles. In general, barriers outside the tropics facilitate meridional heat transport by ocean circulation and, if they extend to high latitudes, result in ice-free poles and warmer climates. Opening of gaps in the barrier at high latitudes inhibits meridional heat H_O there, allowing the poles to freeze over. Opening of gaps at low latitudes, by contrast, enhances meridional H_O at all latitudes, leading to warmer poles.

The equilibrium Drake solution most resembles the present climate and has a marked interhemispheric asymmetry: ice is maintained over the pole of the hemisphere in which the high-latitude barrier is opened up. The meridional overturning circulation of the Drake solution is supported by convection in the warm hemisphere (the push) and wind forcing over the open passageway in the cold hemisphere (the pull).

These different ocean circulations result in a wide range in magnitudes of meridional heat transport by the ocean. The total heat transport of the coupled system, however, varies significantly less across the coupled calculations compared to the individual oceanic and atmospheric components, with changes in atmospheric and oceanic heat transport largely, but not completely, compensating one another.

S78 argued that H_T should be independent of the detailed dynamical processes responsible for that transport but depend only on the incoming solar radiation and the mean planetary albedo: the one-term balance of section 3a. We find that in a warm climate in which there is no ice, Stone's result is a useful guide. In cold climates with significant polar ice caps, however, meridional gradients in albedo significantly affect the absorption of solar radiation and need to be included in any detailed calculation or discussion of total heat transport. Because the meridional extent of polar ice caps is sensitive to details of atmospheric and oceanic circulation, these cannot be ignored. The one-term balance does a poor job in capturing H_T when there is significant ice coverage. As ice cover increases, the mean coalbedo decreases but, significantly, the equator–pole gradient in coalbedo increases. Although a

reduction of the mean coalbedo implies a decreased H_T, enhanced albedo gradients increase H_T. Hence, in some cases the one-term balance predicts that H_T will decrease, whereas in fact it increases. A case in point is that of cold climates. Extensive polar ice caps during the Last Glacial Maximum (LGM) suggest a lower mean coalbedo relative to the present climate but also a larger equator–pole gradient in coalbedo. If the effect of the coalbedo gradient were important, the one-term balance might predict the wrong change in H_T for the LGM. In fact, LGM simulations typically yield greater H_T relative to the present (Ganopolski et al. 1998; Shin et al. 2003) despite a decrease in mean planetary coalbedo. See also Budyko (1969), Sellers (1969), and North (1975) for studies with energy balance models that pertain to the connection among ice, albedo, and total heat transport.

Despite its limitations, the series expansion methodology of S78 remains a useful framework for analysis of the total heat transport. Our study suggests that the four-term balance is required for quantitative study, but at the cost of further complication. The one-term balance [Eq. (14)] expresses H_T in terms of s_2 (the equator–pole gradient in incoming solar radiation) and a_0 (the global-mean coalbedo). Given that s_2 is an external parameter and a_0 is a global parameter, the one-term balance provides an estimate of H_T without detailed knowledge of the interior circulation. In this way, the one-term balance could be used as a model for H_T as was done by W05. The four-term balance [Eq. (13)] captures H_T more accurately but requires knowledge of both a_2 and i_2 and hence details of the circulation and radiative–convective balance. S78 observed from the data available to him that the s_0a_2, s_2a_2, and i_2 terms largely cancelled one another in Eq. (13), leaving the one-term balance. However, in our study, both with models and ERBE data, we do not find such a close cancellation and must retain further terms in the expansion. As a result, it is incorrect to say that H_T is determined entirely by external factors, and we must resort to a more complex description. Furthermore, we are not left with a simple model for H_T.

Nevertheless, in our Ridge and EqPas calculations, it is quite remarkable how insensitive H_T is to the starkly different H_O profiles brought about by the differences in ocean basin geometry. The atmosphere is seemingly able to carry poleward whatever energy is demanded of it. This is especially evident in comparing Ridge and EqPas, which yield H_T that are indistinguishable despite marked differences in H_O (Fig. 10). It is also interesting to note that major differences in climate can exist even in the presence of virtually identical H_T. For example, surface air temperatures at high latitudes in Ridge and EqPas span 5°C (Fig. 4). Even if H_T were to remain constant, a repartitioning of heat transport between the two fluids could still have an important impact on the surface climate. For example, the possibilities of high H_O in the Eocene (Barron 1987) or diminished Northern Hemisphere H_O due to a diminution in Atlantic meridional overturning (Broecker 1997) could be very important for the surface climate.

Finally, it is worth pointing out that the differences in H_T between a warm climate and a cold climate need not be large. For example, comparing Aqua (cold) and Ridge (warm), the peak in H_T differs by only 0.5 PW, even though the climates are starkly different. Given that estimates of the uncertainty in the present climate H_T are around ± 1 PW (Carissimo et al. 1985; W05), this suggests that getting the total heat transport correct is a necessary but not sufficient test of climate models. A similar point is made by S78. Simulated climates with differences in H_T that are on the order of measurement errors can be very dissimilar.

APPENDIX

Two-Box Model of Total Heat Transport

As a pedagogical exercise that parallels the Legendre polynomial expansion approach described in section 3,
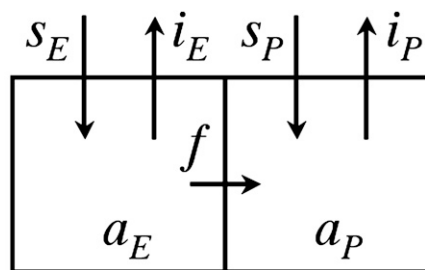
FIG. A1. Configuration of the two-box model. The hemisphere is divided into two equal-area regions separated at $x = 0.5$ ($\phi = 30°$). The incoming solar radiation s, coalbedo a, and OLR i are defined for the equatorial (E) and poleward (P) boxes, with f being the total meridional heat transport between them.

TABLE A1. Terms (nondimensional) in the two-box model (described in the appendix) for the northern hemispheres of Aqua and Ridge and both hemispheres of Drake from Eq. (19). The last two columns compare f (dimensionalized back to H_T in PW) from the two-box model with the fully coupled model. Results from EqPas are almost identical to Ridge and are not shown.

	$-\Delta s\bar{a}$	$-\bar{s}\Delta a$	$-\frac{1}{2}\Delta s\Delta a$	$+\Delta i$	Sum	Two-box model H_T at 30° (PW)	Coupled model H_T at 30° (PW)
Aqua NH	0.240	0.086	−0.016	−0.021	0.289	6.30	6.25
Ridge NH	0.249	0.023	−0.004	0.002	0.270	5.88	5.81
Drake NH	0.250	0.024	−0.004	0.007	0.277	6.03	5.86
Drake SH	0.239	0.087	−0.016	−0.026	0.285	6.21	6.11

here we briefly present a perhaps more physically motivated two-box model of total heat transport: one box represents tropical latitudes, the other middle-to-high latitudes. The configuration of the model is shown in Fig. A1. The hemisphere is divided into two equal-area regions separated at $x = 0.5$ ($\phi = 30°$). We assume that the total heat transport across the equator is zero.

The incoming solar radiation s, coalbedo a, and outgoing longwave radiation i are evaluated for the equatorial (E) and poleward (P) boxes, with f being the total meridional heat transport between them. Integrating Eq. (6) from the pole ($x = 1$; $f = 0$) to $x = 0.5$ yields

$$f = -(\overline{s_P a_P} - \overline{i_P})\Delta x, \qquad (15)$$

where $\Delta x = 0.5$ and the overbar represents the area-averaged values for that box.

Defining

$$\overline{s_P} \equiv \frac{\overline{s_P a_P}}{a_P}$$

and expressing the equatorial and polar box budgets in terms of means and differences, we write:

$$\bar{s} = \frac{1}{2}(\overline{s_E} + \overline{s_P}), \quad \Delta s = \overline{s_P} - \overline{s_E}; \qquad (16)$$

$$\bar{a} = \frac{1}{2}(\overline{a_E} + \overline{a_P}), \quad \Delta a = \overline{a_P} - \overline{a_E}; \quad \text{and} \quad (17)$$

$$\bar{i} = \frac{1}{2}(\overline{i_E} + \overline{i_P}), \quad \Delta i = \overline{i_P} - \overline{i_E}. \qquad (18)$$

Substituting Eqs. (16)–(18) into Eq. (15), and noting that $\bar{s}\bar{a} - \bar{i} \approx \overline{s a} - \bar{i} = 0$, Eq. (15) can be written as

$$f = -\left(\Delta s\bar{a} + \bar{s}\Delta a + \frac{1}{2}\Delta s\Delta a - \Delta i\right)\frac{\Delta x}{2}, \qquad (19)$$

which should be compared to Eq. (13) of the Legendre polynomial expansion model of S78. There is clearly a one-to-one correspondence between the terms, showing that the results of section 3c can also be interpreted in terms of the two-box model presented here.

Table A1 shows the contribution of the four terms on the rhs of Eq. (19) for Aqua, Ridge, and Drake. For Aqua, the $\Delta s\bar{a}$ term remains the largest, but it is smaller relative to Ridge because of the presence of large ice caps and hence a decreased planetary albedo. By virtue of ice caps being located in the polar box, there is now a significant gradient in absorption. In Aqua, the second term representing the gradient in coalbedo is a third the magnitude of the first term. A part is compensated by a stronger (weaker) OLR in the region of strong (weak) absorption (Δi and Δa are of same sign), but overall the strong gradient in coalbedo is concurrent with stronger H_T. In all of the coupled calculations the $\Delta s\Delta a$ term is small. Drake is similar to Ridge in the Northern Hemisphere (the $\Delta s\bar{a}$ term dominates) and similar to Aqua in the Southern Hemisphere (where terms other than $\Delta s\bar{a}$ are also significant). The two-box model also captures the nonantisymmetry of the Drake H_T.

REFERENCES

Adcroft, A., J.-M. Campin, C. Hill, and J. Marshall, 2004: Implementation of an atmosphere–ocean general circulation model on the expanded spherical cube. *Mon. Wea. Rev.,* **132,** 2845–2863.

Barkstrom, B., E. Harrison, G. Smith, R. Green, J. Kibler, and R. Cess, the ERBE Science Team, 1989: Earth Radiation Budget Experiment (ERBE) archival and April 1985 results. *Bull. Amer. Meteor. Soc.,* **70,** 1254–1262.

Barron, E. J., 1987: Eocene equator-to-pole surface ocean temperatures: A significant climate problem? *Paleoceanography,* **2,** 729–739.

Bess, T. D., and G. L. Smith, 1993: Earth radiation budget: Results of outgoing longwave radiation from *Nimbus-7, NOAA-9,* and ERBS satellites. *J. Appl. Meteor.,* **32,** 813–824.

Bjerknes, J., 1964: Atlantic air/sea interaction. *Advances in Geophysics,* Vol. 10, Academic Press, 1–82.

Briegleb, B., P. Minnis, V. Ramanathan, and E. Harrison, 1986: Comparison of regional clear-sky albedos inferred from satellite observations and model computations. *J. Appl. Meteor.,* **25,** 214–226.

Broecker, W., 1997: Thermohaline circulation, the Achilles heel of our climate system: Will man-made CO_2 upset the current balance? *Science,* **278,** 1582–1588.

Bryden, H. L., H. R. Longworth, and S. A. Cunningham, 2005: Slowing of the Atlantic meridional overturning circulation at 25°N. *Nature,* **438,** 655–657.

Budyko, M. I., 1969: The effect of solar radiation variations on the climate of the earth. *Tellus,* **21,** 611–619.

Carissimo, B. C., A. Oort, and T. H. Vonder Haar, 1985: Estimating the meridional energy transports in the atmosphere and ocean. *J. Phys. Oceanogr.,* **15,** 82–91.

Czaja, A., and J. Marshall, 2006: The partitioning of poleward heat transport between the atmosphere and ocean. *J. Atmos. Sci.,* **63,** 1498–1511.

Ellis, J. S., and T. H. Vonder Haar, 1976: Zonal average earth radiation budget measurements from satellites for climate studies. Atmospheric Science Paper 240, Colorado State University, 58 pp.

Frierson, D. M. W., I. M. Held, and P. Zurita-Gotor, 2007: A gray-radiation aquaplanet moist GCM. Part II: Energy transports in altered climates. *J. Atmos. Sci.,* **64,** 1680–1693.

Ganopolski, A., S. Rahmstorf, V. Petoukhov, and M. Claussen, 1998: Simulation of modern and glacial climates with a coupled global model of intermediate complexity. *Nature,* **391,** 351–356.

Gent, P. R., and J. C. McWilliams, 1990: Isopycnal mixing in ocean circulation models. *J. Phys. Oceanogr.,* **20,** 150–155.

Griffies, S. M., 1998: The Gent–McWilliams skew flux. *J. Phys. Oceanogr.,* **28,** 831–841.

Held, I. M., 2001: The partitioning of the poleward energy transport between the tropical ocean and atmosphere. *J. Atmos. Sci.,* **58,** 943–948.

Hotinski, R. M., and J. R. Toggweiler, 2003: Impact of a Tethyan circumglobal passage on ocean heat transport and "equable" climates. *Paleoceanography,* **18,** 1007, doi:10.1029/2001PA000730.

Keith, D. W., 1995: Meridional energy transport: Uncertainty in zonal means. *Tellus,* **47A,** 30–44.

Klinger, B. A., J. Marshall, and U. Send, 1996: Representation of convective plumes by vertical adjustment. *J. Geophys. Res.,* **101** (C8), 18 175–18 182.

Marshall, J., A. Adcroft, C. Hill, L. Perelman, and C. Heisey, 1997a: A finite-volume, incompressible Navier–Stokes model for studies of the ocean on parallel computers. *J. Geophys. Res.,* **102** (C3), 5753–5766.

——, C. Hill, L. Perelman, and A. Adcroft, 1997b: Hydrostatic, quasi-hydrostatic, and nonhydrostatic ocean modeling. *J. Geophys. Res.,* **102** (C3), 5733–5752.

——, and Coauthors, 2001: North Atlantic climate variability: Phenomena, impacts and mechanisms. *Int. J. Climatol.,* **21,** 1863–1898.

——, A. Adcroft, J.-M. Campin, C. Hill, and A. White, 2004: Atmosphere ocean modeling exploiting fluid isomorphisms. *Mon. Wea. Rev.,* **132,** 2882–2894.

——, D. Ferreia, J.-M. Campin, and D. Enderton, 2007: Mean climate and variability of the atmosphere and ocean on an aquaplanet. *J. Atmos. Sci.,* **64,** 4270–4286.

Molteni, F., 2003: Atmospheric simulations using a GCM with simplified physical parameterizations. Part I: Model climatology and variability in multi-decadal experiments. *Climate Dyn.,* **20,** 175–191.

North, G. R., 1975: Theory of energy-balance models. *J. Atmos. Sci.,* **32,** 2033–2043.

O'Gorman, P. A., and T. Schneider, 2007: The hydrological cycle over a wide range of climates simulated with an idealized GCM. *J. Climate,* **21,** 3815–3832.

Pierrehumbert, R. T., 2002: The hydrologic cycle in deep-time climate problems. *Nature,* **419,** 191–198.

Redi, M. H., 1982: Oceanic isopycnal mixing by coordinate rotation. *J. Phys. Oceanogr.,* **12,** 1154–1158.

Sellers, W. D., 1969: A global climatic model based on the energy balance of the earth–atmosphere system. *J. Appl. Meteor.,* **8,** 392–400.

Shin, S.-I., Z. Lui, B. Otto-Bliesner, E. C. Brady, J. E. Kutzbach, and S. P. Harrison, 2003: A simulation of the Last Glacial Maximum climate using the NCAR-CCSM. *Climate Dyn.,* **20,** 127–151.

Smith, R. S., Ocean circulations and climate dynamics under idealised continental configurations in a coupled ocean–atmosphere model. Ph.D. thesis, University of Southampton, 199 pp.

Stone, P. H., 1978: Constraints on dynamical transports of energy on a spherical planet. *Dyn. Atmos. Oceans,* **2,** 123–139.

Toggweiler, J. R., and H. Bjornsson, 2000: Drake Passage and paleoclimate. *J. Quat. Sci.,* **15,** 319–328.

Trenberth, K. E., and J. M. Caron, 2001: Estimates of meridional atmosphere and ocean heat transports. *J. Climate,* **14,** 3433–3443.

Warren, B. A., 1999: Approximating the energy transport across oceanic sections. *J. Geophys. Res.,* **104** (C4), 7915–7920.

Winton, M., 2000: A reformulated three-layer sea ice model. *J. Atmos. Oceanic Technol.,* **17,** 525–531.

Wunsch, C., 2005: The total meridional heat flux and its oceanic and atmospheric partition. *J. Climate,* **18,** 4374–4380.

——, and P. Heimbach, 2006: Estimated decadal changes in the North Atlantic meridional overturning circulation and heat flux 1993–2004. *J. Phys. Oceanogr.,* **36,** 2012–2024.